Light-controlled flows in active fluids

Julien Dervaux, Marina Capellazzi Resta, Philippe Brunet

Light-controlled flows in active fluids

Julien Dervaux,[1] Marina Capellazzi Resta,[1] and Philippe Brunet[1]
[1] *Laboratoire Matière et Systèmes Complexes, Universitée Denis Diderot, Paris, France*
(Dated: October 22, 2019)

Many photosynthetic micro-organisms are able to detect light and move toward optimal intensities. This ability, known as phototaxis, plays a major role in ecology by affecting natural phytoplankton mass transfers and has important applications in bioreactor and artificial microswimmers technologies. Here we show that this property can be exploited to generate macroscopic fluid flows using a localized light source directed toward shallow suspensions of phototactic micro-organisms. Within the intensity range of positive phototaxis, algae accumulate beneath the excitation light where collective effects lead to the emergence of radially symmetric convective flows. These flows can thus be used as hydrodynamic tweezers to manipulate small floating objects. At high cell density and layer depth, we uncover a new kind of instability wherein the viscous torque exerted by self-generated fluid flows on the swimmers induces the formation of traveling waves. A model coupling fluid flow, cell concentration and orientation finely reproduces the experimental data.

In order to survive in fluctuating heterogeneous environments, micro-organisms have developed a wide array of mechanisms allowing them to move in external gradients. Directed motions can rely on biochemical circuits that detect and process external physico-chemical cues to bias micro-organism motion toward or away from those signals (chemotaxis, thermotaxis, phototaxis, etc), but can also rely on passive physical forces. Asymmetry in the cell mass distribution [1, 2] can induce a motion along the direction of gravity (gravitaxis) and shear flows affect micro-swimmer orientation, a mechanism known as gyrotaxis [3] that may lead to the formation of thin concentrated layers in natural aquatic environments [4]. Applying external gradients to dilute suspensions of micro-organisms allows to quantify the response of individual micro-organisms to external stimuli [5–9]. At higher density, cell suspensions also exhibit fascinating nontrivial collective responses to these external gradients, unseen at the single-cell level, such as front propagation, pattern formation [10] or the generation of meso- and macroscopic flows which affect micro-organisms transport.

While mesoscopic flows originate from hydrodynamic or steric interactions between cells in dense suspensions [11], independently of any externally applied field, macroscopic self-generated convective flows ("bioconvection") arise from density differences between cells and their surrounding fluid. Spatial gradients of cell concentration create differential buoyancy forces that drive large scale flows. However, although bioconvection is an appealing mechanism to generate or enhance mixing in biological suspensions [12, 13], a major challenge in bioreactor technologies, but also to prevent biofouling and even to harvest micro-organisms [14], its control remains elusive. Indeed, bioconvection studies so far have been essentially restricted to pattern selection, appearing spontaneously in concentrated layers, where a vertical (in the direction of gravity) cell concentration gradient develops as a result of the upward-swimming induced by negative gravitaxis [15–18], oxygen consumption [19–21] or a combination of several fields [22–29].

Here we use light to induce and control the collective swimming of *Chlamydomonas reinhardtii* (CR) cells, a motile phototactic micro-algae. This collective dynamics lead to the emergence of macroscopic fluid flows at scales larger than a thousand times the size of a single micro-organism at cell concentrations lower than those required for both mesoscopic and spontaneous bioconvective macroscopic flows to occur. Then, we demonstrate that this light-induced flow can act as tweezers to manipulate small beads floating at the free surface of the suspension.

By imposing a horizontal light gradient in a shallow CR suspension, we generate an inhomogeneous concentration field that becomes maximal around the location of the laser spot. From these data, we are able for the first time to quantify the average drift velocity of CR cells subjected to light intensity gradients. Above a critical cell concentration or suspension depth, we uncover a new kind of instability, bearing some resemblance with hydrothermal waves, in which waves of concentrated algae propagate away from the light source. We propose a mechanism where the flow vorticity of the main convective flow, coupled to cell gyrotaxis, focuses the microswimmers in a thin concentrated layer within the bulk of the suspension. At the critical threshold, this layer undergoes an overturning instability, similar to Rayleigh-Taylor instability [30, 31], in which descending plumes are advected by the primary flow to generate traveling waves. We then develop a continuous model coupling phototaxis, cell orientation and cell concentration-driven fluid flows. Extensive numerical simulations are rigorously compared to experimental data and provide a quantitative validation of the model. The good agreement between numerics and experiments is very promising to predict the dynamics of active fluids in more complex geometries.

CR cells are $\sim 10\mu$m wide spheroids that swim with two flagella moving in a breast-stroke fashion [32], pro-

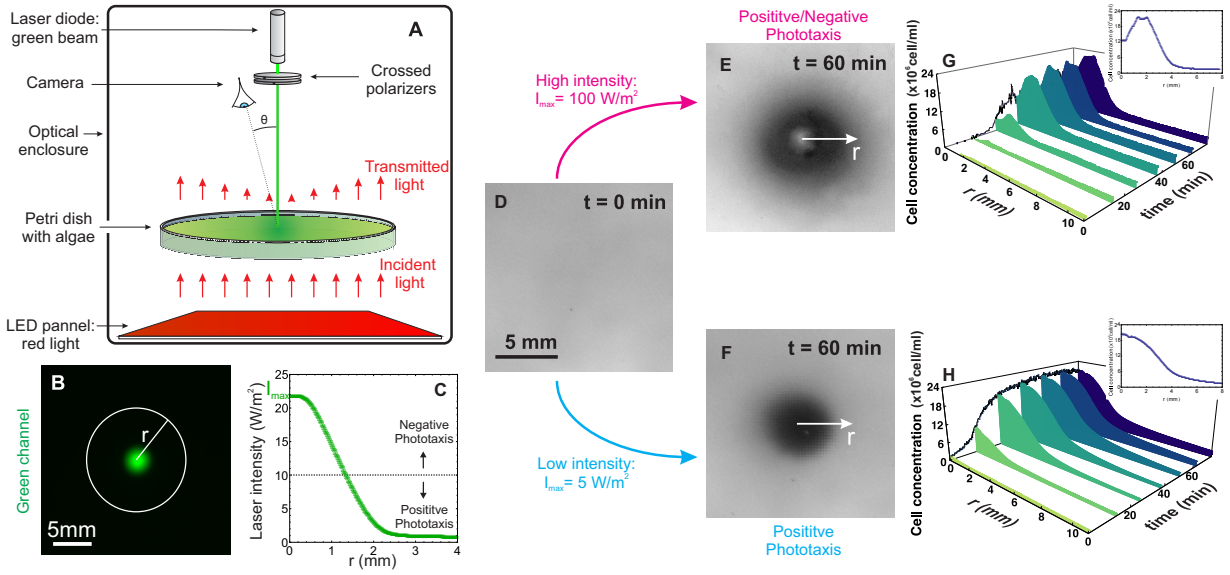

FIG. 1. Experimental setup used to investigate the interaction between light and algae. A: Experimental setup (see Materials and Methods). The shape of the laser beam is acquired in the green channel (B) and converted to a light intensity profile (C). D-F: typical images captured on the red channel of the detector, starting from the same homogeneous initial condition (C) at low thickness ($H = 1.51$mm) and cell concentration ($c_0 = 0.69 \cdot 10^6$cell/ml). In E, the maximum light intensity $\mathrm{I_{max}}$ is 100 W/m^2 and both positive and negative phototaxis are observed. In F, $\mathrm{I_{max}} = 5$ W/m^2 and only positive phototaxis is observed. In both cases, the cell concentration field remains axisymmetric. G-H: the cell concentration averaged along $\theta = [0; 2\pi]$ reaches a steady state within approximately 30 min for both high (G) and low (H) intensities. After one hour, the cell concentration at the center of the spot started to decrease slightly, indicating that algae may be slowly acclimating to the light conditions. The insets in G and H show the corresponding cell concentration profiles at $t = 60$ min. The dip in concentration at the center of the beam in the inset of panel G is the signature of negative phototaxis.

pelling the cell at mean velocity $\sim 100\mu$m/s. The cell density, slightly larger than that of water, equals $\rho_{\mathrm{cell}} = 1050$ kg/m^3. CR uses a photosensitive stigma to detect light gradients [33]. Being widely used as a model organism in biology [34] and biophysics [35], CR also has important applications in biofuel [36], biohydrogen [37] and valuable pharmaceutical molecules [38, 39] productions.

To investigate the response of CR to light, a leveled Petri dish was filled with a thin layer of algal suspension and carefully confined in a dark enclosure, as illustrated in Fig. 1 A. A green laser beam lights the center of the plate and, in order to observe the micro-organisms, a LED panel with a red filter was placed below the Petri dish. The intensity of the light transmitted through the algal suspension was then converted, after calibration, into a local concentration, averaged across the layer height. We first conducted a set of experiments at thin algal layer and measured the height-averaged concentration as a function of space and time. Starting from a homogeneous initial condition (Fig. 1D), Fig. 1 E and F illustrate two typical experiments showing the aggregation of the cells below the laser spot for two different values of the maximum light intensity $\mathrm{I_{max}}$ at the center of the laser beam. In both cases, the cell concentration fields were axisymmetric (Fig. 1 E and F) and reached a steady state in approximately 30 min (Fig. 1 G and H). At high light intensity ($\mathrm{I_{max}} = 100$ W/m^2), cells swam away from the center of the beam (negative phototaxis) and localized in a ring-like area around the beam (Fig. 1-E), where the beam intensity was lower (positive phototaxis). To find the crossover between positive and negative phototaxis, crossed polarizers were placed on the beam path to reduce the maximum light intensity. Crossover occurred for a light intensity of ~ 10 W/m^2. The light intensity was thus fixed at $\mathrm{I_{max}} = 5$ W/m^2 such that only positive phototaxis (Fig. 1 F) occurred and the same settings were used in all experiments.

We then investigated the effect of the initial concentration of algae c_0 and thickness H of the fluid layer. Several concentration profiles are shown in Fig. 2 A-D and their overall shapes did not change significantly when varying the control parameters. However, as shown in Fig. 2 E, the dependance of the maximum cell concentration c_{max} at the center of the light beam with c_0 (at fixed H) reveals two distinct regimes. For $c_0 \lesssim 0.6{\cdot}10^6$cell/ml, c_{max} increases linearly with c_0 as : $c_{\mathrm{max}} \sim 25 c_0$. For larger c_0 ($\gtrsim 0.6 \cdot 10^6$cell/ml), c_{max} becomes weakly dependent on c_0 (Fig. 2 A), increasing 10 times slower than in the first low-c_0 regime. On the other hand, in this regime c_{max} decreases with increasing height (at a fixed c_0), as can be seen in Fig. 2 F, with the scaling $c_{\mathrm{max}} - c_0 \sim H^{-0.8}$.

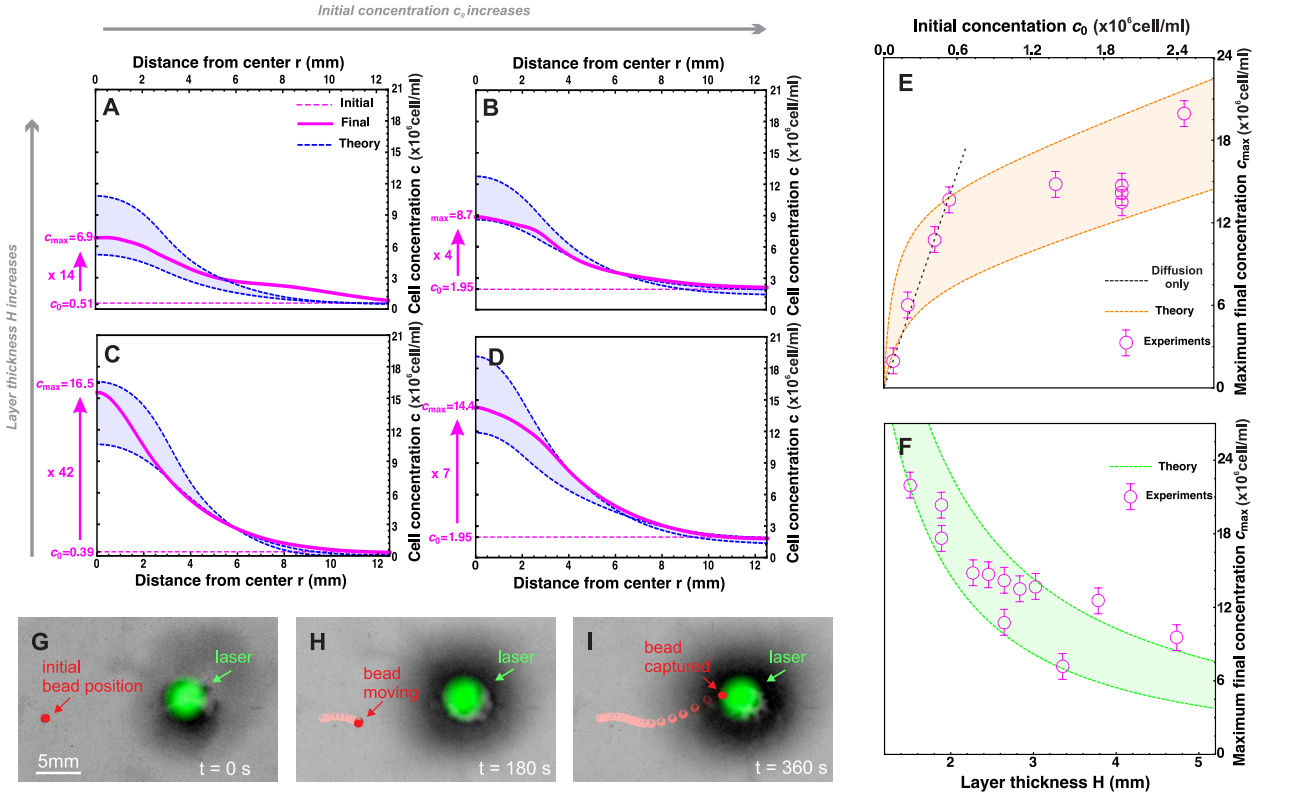

FIG. 2. Effect of thickness and initial concentration on the concentration profiles. A-D: Concentration profiles for different values of the control parameters. A: $c_0 = 0.51 \cdot 10^6$cell/ml and $H = 3.41$mm. B: $c_0 = 1.95 \cdot 10^6$cell/ml and $H = 3.22$mm. C: $c_0 = 0.39 \cdot 10^6$cell/ml and $H = 1.89$mm. D: $c_0 = 1.95 \cdot 10^6$cell/ml and $H = 2.46$mm. The magenta dashed lines (resp. magenta solid) are the experimental profiles in the initial (resp. final) states. The blue dashed lines are the theoretical curves corresponding to phototactic parameters $\chi = 0.8 \cdot 10^{-7}$ m^4/J (where the J stands for Joule) for the lower curves and $\chi = 1.4 \cdot 10^{-7}$ m^4/J for the higher curves. These values correspond to plus or minus one standard deviation around the fitted value $\chi = 1.1 \cdot 10^{-7}$ m^4/J. The quantity χ is the phototactic parameter relating the drift speed V_s of the algae to the radial light intensity gradient through $V_s = \chi \partial I/\partial r$. The experimental data at low concentration ($c_0 \leq 0.6 \cdot 10^6$cell/ml) were fitted with equation (4) using the least squares method to extract the value of χ. E: Maximum cell concentration as a function of the initial cell concentration c_0 for $H = 2.62$mm. The diffusion-only model (equation (4)) is shown with a black dashed line. F: Maximum cell concentration as a function of the layer thickness for $c_0 = 1.5 \cdot 10^6$cell/ml. In E and F, error bars represent standard deviations between three replicates. G-I: Sequence showing the capture of 800μm glass bead (false-colored in red) floating at the surface of the algal layer ($c_0 = 1.95 \cdot 10^6$cell/ml and $H = 3.61$mm). The bead is deposited onto the surface at $t = 0$ (G) and the convergent flow field at the surface drags the bead toward the stagnation point below the laser spot (H) where it remains trapped (I). The velocity of the bead increased from 20μm/s 15mm away from the center up to 140μm/s near the stagnation point.

Because of the density difference between water and algae, a flow is likely to be generated due to the lateral (horizontal) cell concentration gradient. Indeed, by similar reasoning as in thermally-driven convection of a laterally heated fluid [41, 42], a density gradient orthogonal to the direction of gravity triggers convective flows without any threshold. This contrasts with vertical convection (with a density gradient aligned with gravity) where the amplitude of the density gradient must exceed a critical value above which convection can happen. The presence of convection was indeed confirmed by using 800μm glass beads floating at the free surface of the algal layer, as illustrated in Figs. 2 G-I.

The flow produced by such a density gradient results from a balance between buoyancy, cell diffusion and momentum diffusion. The successive bifurcations that the flow experience can be quantified by the Rayleigh (Ra) number [41] :

$$\mathrm{Ra} = \frac{\rho_0 g \beta H^3 \Delta c}{D \mu} \tag{1}$$

where D is the effective diffusion coefficient of the algae, μ is the viscosity of the cell suspension, ρ_0 the density of the medium in absence of cell, g is the acceleration of gravity, Δc is the amplitude of the lateral concentration gradient and $\beta = (\rho_{\mathrm{ref}} - \rho_0)/(c_{\mathrm{ref}}\rho_0)$ quantifies the relative density difference between cells and the ambient medium (where ρ_{ref} is the density of a suspension at a concentration c_{ref}).

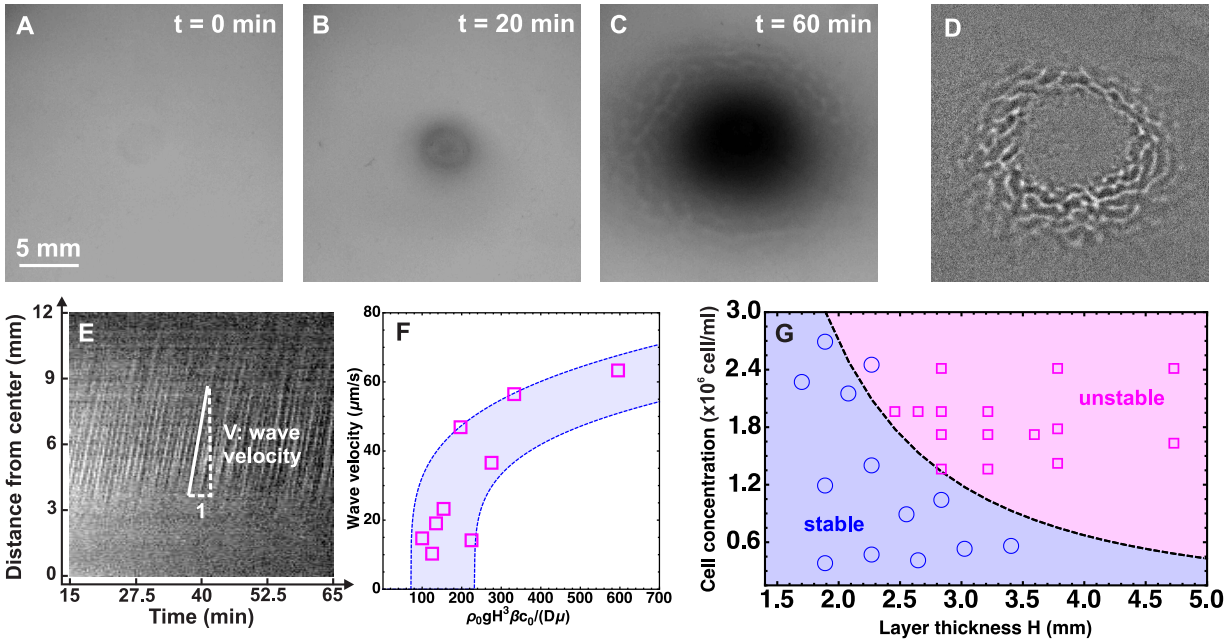

FIG. 3. Formation of unstable patterns above a critical Rayleigh number. A-C: Formation of concentration waves propagating radially in the outward direction. A: the cell concentration field is initially homogeneous (initial concentration $c_0 = 1.95 \cdot 10^6$cell/ml and $H = 3.22$mm). B: after 20 min, cells have started to accumulate beneath the laser spot but the pattern is radially symmetric. C: after 60 min however, waves appears $\sim$ 5mm away from the center and propagate radially away from the concentrated region. D: subtracting the permanent regime (obtained by averaging the images between 60 and 65 min) from image C allows to extract the unstationary component of the concentration field and clearly shows the structure of the waves. E: from these images a kymograph is constructed in the r-t space and allows an accurate measurement of the wave velocity. These velocities are then plotted as a function of the Rayleigh number in panel F. The upper and lower dotted lines are the theoretical curves for $B = 1.4$s and $B = 1$s, respectively. The gyrotactic parameter B is the timescale of algae re-orientation along the direction of the light gradient when the flow is switched off. G: the phase diagram shows the repartition of the stable and unstable regimes in the c_0-H phase space. The dotted line is the marginal stability curve obtained from the numerical resolution of the model (2), (3) and (5) under the incompressibility condition on an axially symmetric domain with no-flux boundary conditions for the cell concentration field and slip (resp. no-slip) condition for the fluid velocity at the top (resp. bottom) surface of the domain (see Materials and Methods). At even higher cell concentration or layer thickness (or, using (1), above a critical Rayleigh number $\mathrm{Ra}_c \sim 1500$), beyond the parameter domain covered in Fig. 3-G, spontaneous bioconvection occurs in the whole cell even in the absence of a light gradient. This threshold value is very close to that reported in a previous study ($\mathrm{Ra}_c \sim 1400$ in [18] for a strain of CR closely related to the strain used in our study) and comparable to the theoretical prediction $\mathrm{Ra}_c \sim 900 - 1800$ that can be obtained from [15] for our system.

Upon further increasing the cell concentration or layer thickness, we observed the formation of unstable patterns, as illustrated in Fig. 3. Starting from a homogenous concentration field (Fig. 3-A), algae accumulate beneath the laser spot. At the beginning of the experiments, the cell concentration monotonically decreases in the radial direction and remains axisymmetric, as in the stable regime (Fig. 3-B). However after 10 to 30 min, the pattern loses its axisymmetry and time invariance (Fig. 3-C). Waves of concentrated micro-organisms appear at the periphery of the concentrated region ($\sim$ 4 mm away from the center of the beam) and propagate away from the concentrated region (Fig. 3-C). These waves appear periodically (with a period of roughly 30 s) as $\sim 0.5 - 1$ mm thick rings of concentrated microswimmers that fragment in the orthoradial direction in domains of irregular width (typically 0.5-5 mm) before the ring is fully detached from the central part. The distance between rings in the radial direction is of the order of the thickness of the rings. The waves propagate radially across a distance of $\sim$ 3mm before vanishing. Although the concentration field is not time-invariant, averaging the pattern over a few periods revealed that the cell distribution could be decomposed into a steady, permanent concentration profile, and an unsteady fluctuating one.

As in the stable, time-invariant regime, the steady component has a well-defined $c_{\max}$ at the center of the laser spot, and the concentration decreases monotonically away from the center. By subtracting this permanent component from each frame, we can extract the non-stationary one (Fig. 3-D). We then plot the light intensity along a radius in this figure as a function of time. The resulting kymograph in the $r - t$ space allows an

accurate determination of the wave velocity (Fig. 3-E). Depending on the thickness H and initial cell concentration c_0, the velocity of the waves varies between 10 to 60 μm/s. These velocities are plotted in Fig. 3-F as a function of the dimensionless number $\rho_0 g\beta H^3 c_0/(D\mu)$. Finally Fig. 3-G presents the phase diagram in the H-c_0 space and shows the parameter domains of the stable and unstable regimes.

We now theoretically analyze the experimental observations. In all generality, cell transport is controlled by convection as well as diffusion, which arises macroscopically from the run-and-tumble-like motion of individual CR cells in the dark. In the presence of a light gradient, phototaxis steers the cells toward or away from the light source [33] and there is an additional phototactic flux. The cell concentration is thus described by the following diffusion-advection equation [26]:

$$\frac{\partial c}{\partial t} = \vec{\nabla}\cdot\Big(\underbrace{D\vec{\nabla}c}_{\text{diffusion}} - \underbrace{cV_s\vec{q}}_{\text{phototaxis}} - \underbrace{c\vec{v}}_{\text{advection}}\Big) \qquad (2)$$

where V_s is the drift speed of the algae due to the radial light intensity gradient, i.e $V_s = \chi\partial I/\partial r$ and $\vec{q}$ is the average orientation of the micro-organisms. The quantity χ is an unknown phototactic parameter that has units of $m^4/(J)$ and we first assume that the phototactic flux $cV_s\vec{q}$ is directed toward the direction of the light gradient, i.e $\vec{q} = \vec{u_r}$. Within the Boussinesq approximation [41], the velocity $\vec{v}$ and pressure p in the incompressible fluid satisfy $\vec{\nabla}\cdot\vec{v} = 0$ and the Navier-Stokes equation:

$$\rho\frac{\partial\vec{v}}{\partial t} = \mu\Delta\vec{v} - \vec{\nabla}p + g\rho_0(1+\beta c)\vec{z} \qquad (3)$$

At very low cell concentration, fluid density differences create minute flows and their contribution to mass transport is negligible compared to diffusion. In this regime, the stationary state is described by the following equation: $D\partial c/\partial r = c\chi\partial I/\partial r$, which is obtained from eq. (2) by removing both convective and time-dependent terms, and assuming that the concentration field only varies in the radial direction. Solving this equation under the constraint of fixed total number of cells yields the maximum cell concentration at the center:

$$c_{max} = c_0\frac{\pi R^2 e^{\chi I_{max}/D}}{\int_0^R \mathrm{d}r e^{\chi I(r)/D}} \text{ (for diffusive transport)} \qquad (4)$$

where R is the radius of the Petri dish. This equation is valid at low concentrations provided that I_{max} remains, as in our experiments, below the intensity threshold where negative phototaxis occurs ($\sim 10\mathrm{W/m^2}$). $c_{\max}$ is indeed, as experimentally observed at low c_0, linearly proportional to c_0 (Figs. 2-E and F). The diffusion coefficient of the algae was obtained by first concentrating the cell using light and then following the relaxation of the cell concentration profile after switching off the light to yield $D = 0.85\pm0.15\cdot10^{-7}\mathrm{m^2/s}$ (see Supplementary Materials). Fitting eq. (4) to the data at low concentration ($c_0 \leq 0.6\cdot10^6$cell/ml) allows a determination of the phototactic coupling parameter $\chi = 1.1\pm0.3\cdot10^{-7}$ m^4/(J). At higher concentrations ($c_0 \geq 0.6\cdot10^6$cell/ml), Figs. 2-E and F show that data depart from this purely diffusive regime and now depend on the thickness H, therefore suggesting that convection becomes significant in this range of concentration. All the other parameters being known (see Materials and Methods), the numerical solution of the theoretical model (2)-(3) that includes convection (together with the incompressibility constraint) has been carried out and indeed shows a good agreement with the experimental data, (Figs. 2A-F).

However, the numerical resolution of this model does not reveal any instabilities in the range of parameters relevant to our experiments. As described in the Supplementary Materials, waves of nutrient concentration or quorum sensing effects cannot explain the formation of these unstable patterns either. The underlying mechanism of the propagating waves observed in Figs. 3A-D has to be sought elsewhere, namely in the coupling between the flow and the cell orientation distribution $\vec{q}$ that was neglected so far. Indeed, because the fluid flow generated by the algae has a non-zero vorticity, it is well known that it induces a rotation of individual cells [44, 45]. When cells have a principal drift direction, in the present case along the orientation $\vec{u_r}$ of the light gradient, cells are rotated away from this preferential orientation. In that case, the hypothesis formulated above stating that the algae mean orientation $\vec{q} = \vec{u_r}$ breaks down. Instead the selection of the orientation $\vec{q}$ results from a balance between the viscous torque and the light intensity gradient that act to align $\vec{q}$ with $\vec{u_r}$ such that $\vec{q}$ satisfies the following differential equation [45]:

$$\frac{\partial\vec{q}}{\partial t} = \frac{1}{2B}\{\vec{u_r} - (\vec{u_r}\cdot\vec{q})\vec{q}\} + \frac{1}{2}\vec{\omega}\times\vec{q} \qquad (5)$$

where B is the timescale of algae re-orientation along the direction $\vec{u_r}$ of the light gradient when the flow is switched off and $\vec{\omega} = \vec{\nabla}\times\vec{v}$ is the flow vorticity. This effect, known as gyrotaxis, was first evidenced for cells drifting due to gravity in a shear flow [3] and, more recently, was also found to occur for CR cells under the influence of a light intensity gradient [46]. An important consequence of gyrotaxis is that cells are focused at the center of a Poiseuille flow when their drift direction is opposite to that of the flow, while they are dispersed in the same flow when the drift velocity goes in the same direction as the fluid flow. In the present case, the radial flow is directed toward the light source in the upper part of the algal suspension while it is directed outward in the lower part of the suspension, as illustrated in Fig.

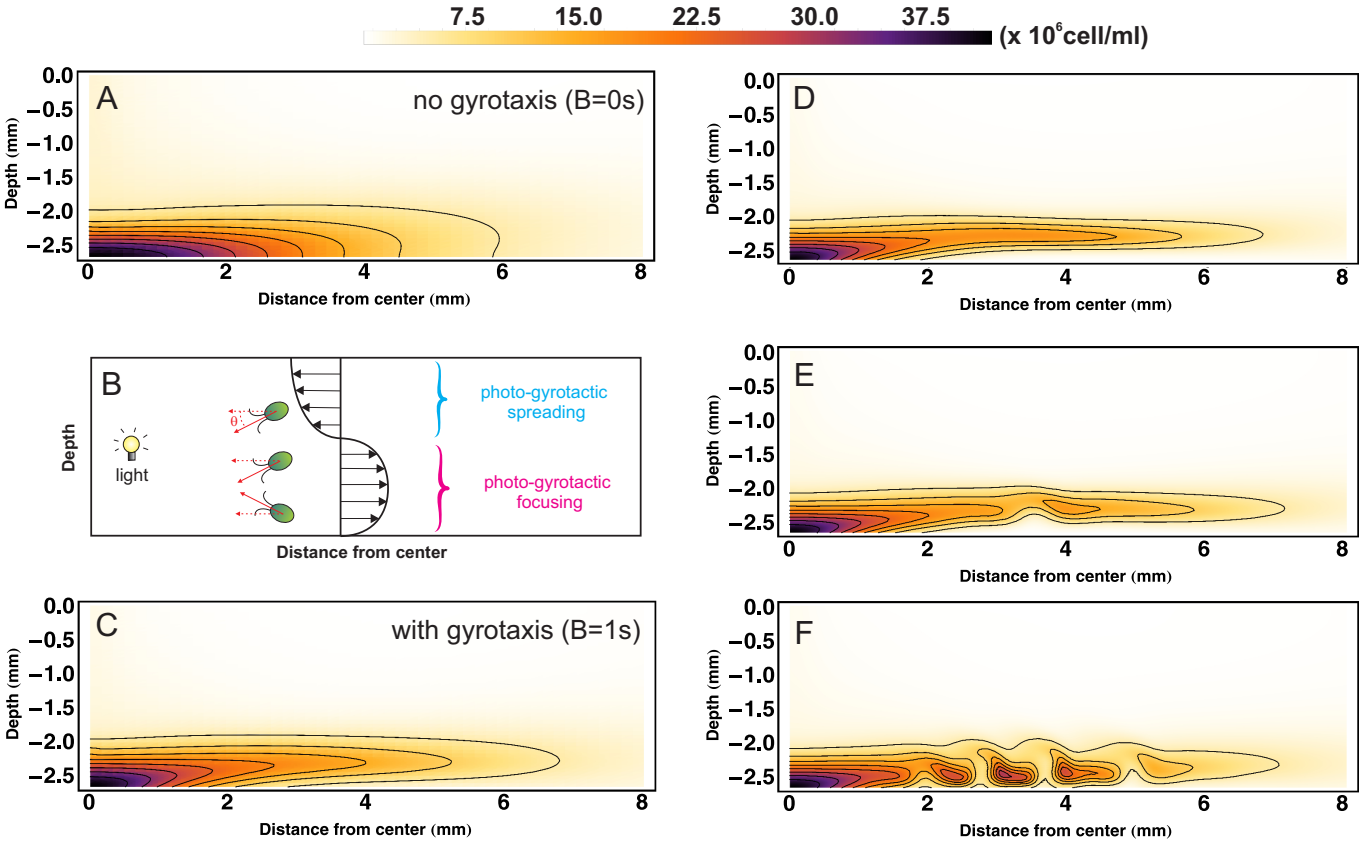

FIG. 4. Underlying mechanism of the instability. A,C,D,E and F: side views of the results from the numerical calculations with color coded cell concentrations. In the stable regime (A and C), starting from an homogeneous state (initial concentration $c_0 = 1.5 \cdot 10^6$cell/ml and $H = 2.51$mm), the system reaches a time independent equilibrium state (here presented after 90 minutes of simulation). A: without gyrotaxis ($B = 0$ s), the algae are concentrated in a dense layer at the bottom of the Petri dish. B: sketch illustrating the fluid flow (indicated with black arrows) generated by the algae. This flow occurs because of both the radial cell concentration gradient and the difference in density between cells and their surrounding fluid. This sketch further illustrates the photo-gyrotactic effect that causes algae to experience an additional drift due to the generated flow: cells in the bottom part of the suspension are focused where the outward radial velocity is maximum while cells in the upper part of the suspension are spread by the inward radial flow. C: with this drift taken into account (using the value $B = 1$ s for the gyrotactic parameter), the algae are also concentrated in a dense layer but above the bottom of the Petri dish. At slightly higher cell concentration ($c_0 = 1.8 \cdot 10^6$cell/ml), the system enters the unstable regime. Panels D to F illustrate three snapshots of the development of this instability (10 s between each snapshots). The dense layer that forms initially (D) first develops a single undulation (E) and further breaks into several clusters of concentrated algae that are advected by the primary flow. Although the present secondary instability occurs in a different geometry, under different boundary conditions and on top of a primary convective flow, let us note that the wavelength of the instability (in the range $1 - 2$ mm) is roughly equals to the distance between the top of the densified layer to the bottom of the Petri dish. This result is consistent with previous theoretical and experimental studies [15, 25, 26].

4-B. We thus expect cells to be concentrated in a dense thin layer just above the bottom of the Petri dish. To confirm this hypothesis, equations (2), (3) and (5) were then solved numerically under the incompressibility constraint (see Materials and Methods). As suggested by previous models [26], the gyrotactic parameter B should be of the order of 1 s. Best fits to the experimental profiles were obtained for $B = 1.2 \pm 0.2$ s (see Fig. 2 A-D) although the value of B (in the range of values we investigated) had only a weak influence on the radial concentration profiles, which were mostly determined by the interplay between phototaxis, diffusion and convection. Furthermore, the model shows good agreement with the experimental data for the dependance of the maximum cell concentration on both the initial cell concentration and the layer thickness (Fig. 2 E and F). Now with the gyrotactic effect taken into account, the model indeed predicts that algae become concentrated in a dense thin layer above the bottom of the Petri dish (Fig. 4-C). The presence of a dense layer was also confirmed by brightfield

microscopy and the divergent radial flow field associated with this layer is in good agreement with the theoretical prediction (see Supplementary Materials). This stratification provides the required mechanism for the instability: above a critical threshold (Fig. 3-D), this dense layer resting on top of a lighter fluid undergoes an overturning - Rayleigh-Taylor [30, 31]- instability (Fig. 4-E) and descending plumes are advected by the primary convective fluid flow (Fig. 4-F). Observed from the top, the advection of these rings indeed produces outward propagating waves. The velocity of these waves was then extracted from the numerical data following the same procedure as for the experimental results and a good agreement was found with no additional fitting parameter (see Fig. 3-G). Furthermore, the model also reproduces very accurately the parameter ranges of the stable and unstable regimes in the phase space (see Fig. 3-E).

In the context of bioreactor technologies, the phototactic property of micro-algae is a promising mechanism for biomass harvesting, a technological limitation in biofuel production. Bioconvective effects arising from cell concentration gradients limit the efficiency of the concentrative power (the maximum value of the ratio c_{max}/c_0) of a light gradient. Our results shows that these effects can be minimized by operating under more confined geometries and our theoretical model can be used to select optimal geometries where the crossover between diffusion and convection occurs. Next, the results presented in our study shows that fluid flows can be easily generated in a suspension of phototactic micro-swimmers with a light-intensity gradient. Using a Gaussian laser spot, which can be seen as the simplest element of a light pattern, a convergent flow field is generated, enabling the trapping of millimeter scale floating beads which might find applications for the non-intrusive manipulation of small objects. Furthermore, the ability of microswimmers to collectively generate fluid flows offers an unique opportunity to control and enhance mixing in biological suspension, which is a major challenge in bioreactor technologies. In contrast with mesoscopic flows, arising in highly dense suspensions, that are coherent over length up to $\sim 10^2$ times the size of the micro-swimmers [11–13], the photo-induced flows presented here are coherent over centimetric length scale ($\sim 10^4$ times the size of the cells), while retaining the same order of magnitude for the velocity field. Also, these flow patterns are larger than those observed in spontaneous bioconvection and occur at smaller global concentration. Due to the versatility of controlling dynamically a light intensity field, much more complex fluid flows could in principle be generated. Such complex light-controlled fluid flows could find important applications in bioreactors, such as the generation of chaos in laminar fluid flows.

On a more fundamental ground, we have uncovered a new type of instability in a suspension of gyrotactic swimmers. Band propagation was first recognized by Adler [48] and was shown to occur when micro-organisms consume an external nutrient, causing them to move from a region of depleted nutrient toward a region rich in nutrients [48]. Similar wave propagation can also be observed if a chemo-attractant is secreted and consumed by the micro-organisms themselves [49, 50]. The properties (existence criterion, dynamics, stability) of these propagating waves are the subject of a vast literature in physics and applied mathematics [10]. In all these cases, micro-organisms behave as diffusing particles and band propagation occurs as a result of the coupled diffusion between the micro-organisms and one, or more, external driving fields. In the present case however, the instability is purely hydrodynamics in nature. In this new kind of instability, micro-swimmers themselves generate a macroscopic flow that couple to their orientation. This feedback triggers an overturning secondary instability that is advected by the primary fluid flow. This mechanism further illustrates the richness of the nonlinear physics controlling the behavior of active fluids.

Acknowledgments

We are indebted to our late colleague F. Rappaport and would like to thank S. Bujaldon from IBPC Institute, Paris, for having provided the strains of *Chlamydomonas reinhardtii* and for their kind and helpful advices to grow cultures. This project is funded by the program Emergence(s) of the City of Paris. We thank Yves Couder, as well as anonymous reviewers, for their critical reading of the manuscript.

Author contributions

Conceived and designed the experiments: JD PB. Performed the experiments: JD MCR. Analyzed the data: JD PB. Contributed reagents/materials/analysis tools: JD PB. Wrote the paper: JD PB.

[1] Roberts, A. M. Geotaxis in motile micro-organisms. *J. Expl Biol.* **53**, 687-699 (1970).

[2] Wager, H. On the effect of gravity upon the movements and aggregation of *Euglena viridis* and other micro-organisms. *Phil. Trans. R. Soc. Lond. B* **201**, 333-390 (1911).

[3] Kessler, J. O. Hydrodynamic focusing of motile algal cells. *Nature* **313**, 208-210 (1985).

[4] Durham, W. M., Kessler, J. O. & Stocker, R. Disruption of vertical motility by shear triggers formation of thin phytoplankton layers. *Science* **323**, 1067-1070 (2009).

[5] Adler, J., Hazelbauer, G. L. & Dahl M. M. Chemotaxis toward sugars in *Escherichia coli. J. Bacteriol.* **115**(3), 824-847 (1973).

[6] Barbara, G. M. & Mitchell, J. G. Bacterial tracking of motile algae. *FEMS Microbiol. Ecol.* **44**(1), 79-87 (2003).

[7] Barbara, G. M. & Mitchell, J. G. Marine bacterial organisation around point-like sources of amino acids. *FEMS Microbiol. Ecol.* **43**(1), 99-109 (2003).

[8] Adler, J. Chemoreceptors in bacteria. *Science* **166**, 1588-1597 (1969).

[9] Giometto, A., Altermatt, F., Maritan, A., Stocker, R. & Rinaldo, A. Generalized receptor law governs phototaxis in the phytoplankton *Euglena gracilis*. *Proc. Natl. Acad. Sci. USA*, 7045-7050 (2015).

[10] Brenner, M. P., Levitov, L. S. & Budrene, E. O. Physical mechanisms for chemotactic pattern formation by bacteria. *Biophys. J.* **74**, 1677-1693 (1998).

[11] Koch, D. L. & Subramanian, G. Collective hydrodynamics of swimming microorganisms: living fluids. *Annu. Rev. Fluid Mech.* **43**, 637-659 (2011).

[12] Kurtuldu, H., Guasto, J. S., Johnson, K. A. & Gollub, J. P. Enhancement of biomixing by swimming algal cells in two-dimensional films. *Proc. Natl. Acad. Sci. USA* **108**, 10391-10395 (2011).

[13] Wilhelmus, M. M. & Dabiri, J. O. Observations of large-scale fluid transport by laser-guided plankton aggregations. *Phys. Fluids* **26**, 101302 (2014).

[14] Bees, M. A. & Croze, O. A. Mathematics for streamlined biofuel production from unicellular algae. *Biofuels* **5**, 53-65 (2014).

[15] Childress, S., Levandowksy, M. & Spiegel, E. A. Pattern formation in a suspension of swimming micro-organisms: equations and stability theory. *J. Fluid Mech.* **63**, 591-613 (1975).

[16] Pedley, T. J., Hill, N. A. & Kessler, J. O. The growth of bioconvection patterns in a uniform suspension of gyrotactic micro-organisms. *J. Fluid Mech.* **195**, 223-237 (1988).

[17] Pedley, T. J. & Kessler, J. O. Hydrodynamic phenomena in suspensions of swimming micro-organisms. *Annu. Rev. Fluid Mech.* **24**, 313-358 (1992).

[18] Yamamoto, Y., Okayama, T., Sato, K. & Takaoki, T. Relation of Pattern Formation to External Conditions in the Flagellate *Chlamydomonas reinhardtii*. *Eur. J. Protistol.* **28**, 415-420 (1992).

[19] Janosi, I. M., Kessler, J. O. & Horvath, V. K. Onset of bioconvection in suspensions of *Bacillus subtilis*. *Phys. Rev. E* **58**, 4793-4800 (1998).

[20] Dombrowski, L., Cisneros, L., Chatkaew, S., Goldstein, R. E. & Kessler, J. O. Self-concentration and large-scale coherence in bacterial dynamics. *Phys. Rev. Lett.* 93, 098103 (2004).

[21] Tuval, I., Cisneros, L., Dombrowski, C., Wolgemuth, C.W., Kessler, J.O. & Goldstein, R.E. Bacterial swimming and oxygen transport near contact lines. *Proc. Natl. Acad. Sci. USA* **102**, 2277-2282 (2005).

[22] Croze, O. A., Ashraf, E. E. & Bees, M. A. Sheared bioconvection in a horizontal tube. *Phys. Biol.* **7**, 046001 (2010).

[23] Ghorai, S., Panda, M. K. & Hill, N. A. Bioconvection in a suspension of isotropically scattering phototactic algae. *Phys. Fluids* **22**, 071901 (2010).

[24] Suematsu, N. J., Awazu, A., Izumi, S., Noda, S., Nakata, S. & Nishimori, H. Localized bioconvection of *Euglena* caused by phototaxis in the lateral direction. *J. Phys. Soc. Jap.* **80**, 064003 (2011).

[25] Williams, C. R. & Bees, M. A. A tale of three taxes: photo-gyro-gravitactic bioconvection, *J. Exp. Biol.* **214**, 2398-2408 (2011).

[26] Williams, C. R. & Bees, M. A. Photo-gyrotactic bioconvection. *J. Fluid Mech.* **678**, 41-86 (2011).

[27] Karimi, A. & Ardekani A. M. Gyrotactic bioconvection at pycnoclines. *J. Fluid Mech.* **733**, 245-267 (2013).

[28] Shoji, E., Nishimori, H., Awazu, A., Izumi, S. & Lima, M. Localized bioconvection patterns and their initial state dependency in *Euglena gracilis* suspensions in an annular container. *J. Phys. Soc. Jap.* **83**, 043001 (2014).

[29] Vincent, R. & Hill, N. Bioconvection in a suspension of phototactic algae. *J. Fluid Mech.* **327**, 343-371 (1996).

[30] Lord Rayleigh, Scientific papers (Cambridge University Press, Oxford, 1900) Vol. II.

[31] Taylor, G.I. The instability of liquid surfaces when accelerated in a direction perpendicular to their planes. I *Proc. R. Soc. London Ser. A* **201**, 192-196 (1950).

[32] Polin, M., Tuval, I., Drescher, K., Gollub, J. P. & Goldstein, R. E. *Chlamydomonas* swims with two gears in a eukaryotic version of run-and-tumble locomotion. *Science* **325**, 487-490 (2009).

[33] Bennett, R. R. & Golestanian, R. A steering mechanism for phototaxis in *Chlamydomonas*. *J. R. Soc. Interface* **12**, 20141164 (2015).

[34] Harris, E. H. The *Chlamydomonas* sourcebook (Academic Press, Oxford, 2009), Vol. 1.

[35] Goldstein, R. E. Green algae as model organisms for biological fluid dynamics. *Annu. Rev. Fluid Mech.* **47**, 343-375 (2015).

[36] Siaut, M., Cuiné, S., Cagnon, C., Fessler, B., Nguyen, M. *et al.* Oil accumulation in the model green alga *Chlamydomonas reinhardtii*: characterization, variability between common laboratory strains and relationship with starch reserves. *BMC Biotechnol.* **11**, 7 (2011).

[37] Melis, A., Zhang, L., Forestier, M. & Ghirardi, M. L. Sustained photobiological hydrogen gas production upon reversible inactivation of oxygen evolution in the green alga *Chlamydomonas reinhardtii*. *Plant Physiol.* **122**, 127-136 (2000).

[38] Almaraz-Delgado, A. L., Flores-Uribe, J., Pérez-España, V. H., Salgado-Manjarrez, E. & Badillo-Corona, J. A. Production of therapeutic proteins in the chloroplast of *Chlamydomonas reinhardtii*. *AMB Express* **4**, 57 (2013).

[39] Rasala, B. A. & Mayfield, S. P. Photosynthetic biomanufacturing in green algae; production of recombinant proteins for industrial, nutritional, and medical uses. *Photosynth. Res.* **123**, 227-239 (2014).

[40] Rafaï, S., Jibuti, L. & Peyla, P. Effective viscosity of microswimmer suspensions. *Phys. Rev. Lett.* **104**, 098102-098105 (2010).

[41] Turner, J. S. Buoyancy effects in fluids, (Cambridge University Press, London, 1973).

[42] Riviere, D., Selva, B., Chraibi, H., Delabre, U. & Delville, J. -P. Convection flows driven by laser heating of a liquid layer. *Phys. Rev. E* **93**, 023112 (2016).

[43] Birikh,R. V. On thermocapillary convection in a horizontal layer of a liquid. *J. Appl. Mech. Tech. Phys.* **7**, 43-44 (1966).

[44] Jeffery, G. B. The motion of ellipsoidal particles immersed in a viscous fluid. *Proc. Roy. Soc. A* **102**, 161-179 (1922).

[45] Leal, L. G. & Hinch, E. The rheology of a suspension of nearly spherical particles subject to Brownian rotations.

J. Fluid Mech. **55**, 745-765 (1972).
[46] Garcia, X., Rafaï, S. & Peyla, P. Light control of the flow of phototactic microswimmer suspensions. *Phys. Rev. Lett.* **110**, 138106 (2013).
[47] Salman, H., Zilman, A., Loverdo, C., Jeffroy, M. & Libchaber, A. Solitary modes of bacterial culture in a temperature gradient. *Phys. Rev. Lett.* **97**, 118101 (2006).
[48] Adler, J. Chemotaxis in bacteria. *Science* **153**, 708-716 (1966).
[49] Budrene, E. O. & Berg, H. Complex patterns formed by motile cells of *Escherichia coli*. *Nature* **349**, 630-633 (1991).
[50] Budrene, E.O. & Berg, H. Dynamics of formation of symmetrical patterns by chemotactic bacteria. *Nature* **376** 49-53 (1995).

MATERIALS AND METHODS

Strains and culture conditions

We used the strain CC124$^-$ of *Chlamydomonas reinhardtii*. CR uses a photosensitive stigma to detect light gradients [33]. Light-induced Ca^{2+}-carried photocurrents cause a depolarization of the membrane which differentially modulates the beating amplitude to the two flagella, thereby steering the cell toward or away from the light source. Above a critical membrane depolarization (or wavelength-dependent critical light intensity), opening of voltage-sensitive Ca^{2+} channels causes a massive calcium influx that triggers the photophobic response and alters the flagellar beating mode.

The algae were kept on HSA medium agar plate. For experiments, algae were propagated in liquid HSA medium on an orbital shaker in an incubator at 25° on a 12h/12h bright/dark light cycle to optimize cell uniformity and motility. Cells were used between 48h and 72h after inoculation in liquid medium to ensure reproducibility of the phototactic response. Algae were left 1h under dim red light before being used in experiments. Experiments at low cell concentrations were performed by diluting a culture of algae with an aliquot of supernatant obtained by centrifuging another aliquot of the same culture at 5000g for 10 min and discarding the cells. Cell counting was performed with a Malassez cell on an inverted microscope and gave a concentration of $5\pm1\cdot10^{-12}$ mol/m^3 at an optical density $OD_{580} = 1$. Using an average cell volume of 500μm^3, this is equivalent to a volume fraction of $\sim 1.5 \cdot 10^{-3}$.

To further establish that fluid flows were induced by the cell concentration gradient, several control experiments were also performed with either: *i)* culture medium only, *ii)* culture supernatant (containing waste products and secondary metabolites) and *iii)* heat-killed cells. In all these cases, no flow was observed, therefore ruling out laser-induced thermal convection as well as Marangoni flows as possible mechanisms. Experiments with heat-killed cells were performed on cultures kept at 100°C for 5 min.

Experimental setup and data acquisition

A leveled Petri dish (inner diameter 84mm) was filled with a layer of algal suspension and, to minimize cell adhesion to the boundaries, this suspension was left undisturbed in the dark for 30 min before being discarded. The Petri dish was then washed with distilled water before being filled again with a thin layer of algal suspension and then carefully confined in a dark enclosure. A green (532nm) Gaussian laser beam (4.5mW, Thorlabs , Germany) was directed toward the center of the plate and the intensity of the beam was calibrated using a luxmeter. In

order to observe the micro-organisms, a large LED panel with a red filter (acting as a highpass filter with a cutoff at $\sim$ 610 nm) was placed below the Petri dish and the intensity of the light transmitted through the algal suspension was recorded with a Nikon D700 digital camera equipped with a Zeiss objective. After calibration, the transmitted light intensity was converted into a cell concentration. The intensity-concentration conversion was carried out in Mathematica and image analysis for wave velocity determination was performed with the ImageJ software. In order to check for attraction toward the red panel, we also ran a control experiment with the LED panel turned off using only the green laser beam. After one hour in the dark, the LED panel was turned on and no difference could be seen on the cell concentration profile obtained with the LED panel on, thus showing that the red light had no distinguishable effect on the cell migration in our experimental setup.

Numerical simulations

The density ρ_0 and the viscosity μ are taken to be those of water at 25°C ($\rho_0 = 997$ kg/m^3 and $\mu = 0.89$ mPa.s). The cell density is ~ 1050 kg/m^3, thus giving a $\beta = 1.610^7$ m^3/mol. The diffusion coefficient was measured as mentioned in the text and described in Supplementary Materials and was found to be $D = 0.85 \cdot 10^{-7}$m^2/s. The chemotactic coupling parameter was taken as $\chi = 1.1 \cdot 10^{-7}$ m^4/(J) unless otherwise specified. Because cell volume fractions always remain below 1%, cell-cell interactions can safely be neglected [40] and we assume that the material parameters χ and D are independent of the cell concentration. Equations (2), (3) and (5), together with incompressibility condition, were then solved numerically using Comsol Multyphysics 5.0 on an axially symmetric domain together with no-flux boundary conditions for the cell concentration field and slip and no-slip conditions for the fluid velocity respectively at the top and bottom surface of the domain. A mesh with at least 150 000 elements was used and simulations were run on a 2.3 GHz QuadCore computer with 16 GB of memory.

Data Availability Statement

The data that support the plots within this paper and other findings of this study are available from the corresponding author upon request.